International Symposium
On Turbulence and Shear Flow
Phenomena (TSFP-9)
June 30 - July 3, 2015 *Melbourne, Australia*

PARAMETRIC ANALYSIS OF FLOW OVER SINUSOIDAL RIBLETS

Kie Okabayashi
Next Generation Aeronautical Innovation Hub Center
Aircraft Systems Research Team
Japan Aerospace Exploration Agency (JAXA)
7-44-1 Jindaiji-Higashimachi, Chofu, Tokyo
182-8522, Japan
okabayashi.kie@jaxa.jp

Yuki Yamada
Graduate School of System Design
Tokyo Metropolitan University
6-6 Asahigaoka, Hino, Tokyo
191-0065, Japan
yamada-yuki@ed.tmu.ac.jp

Masahito Asai
Graduate School of System Design
Tokyo Metropolitan University
6-6 Asahigaoka, Hino, Tokyo 191-0065, Japan
masai@tmu.ac.jp

ABSTRACT

Flows over wavy (sinusoidal) riblets are investigated by means of Direct Numerical Simulation (DNS) in order to improve its configuration. Total drag (pressure drag + friction drag) reduction rate is improved in some cases at a maximum reduction rate of -7.8%, while reduction rate of straight riblet is -6.1%. If β, which is defined as $\beta = tan^{-1}(2\pi a/\lambda)$ (a: amplitude, λ: wavelength), is relatively large, friction drag is reduced drastically by spanwise vortices which periodically occur from detachment at the riblet tip. Too large β, however, causes large pressure drag, which offsets friction drag reduction effect. With relatively small β, on the other hand, spanwise vortices which reduces friction drag occurs, but not periodically. Considering total drag reduction, relatively small β seems better.

INTRODUCTION

Attention must be paid for sustainable aviation to improvement of fuel efficiency aiming at the reduction of CO2 emission. Reduction of skin friction drag will contribute significantly to improvement of aerodynamic performance: Friction drag accounts for about half of total drag of aircraft at cruising condition. As is well known, several reduction technique for skin friction drag have been ever proposed. Unfortunately, most of them have difficulties to put into practical use for now, because of technical problems or cost restrictions. Against this background, recently, several research groups have focused renewed attention on riblet as a realizable flow control device. For example, a research group developed an innovative shape-forming method of riblet (Stenzel et al., 2011 etc.). With that method riblet structure is formed simultaneously during painting process. This method will overcome the disadvantage of riblet, such as additional weight that offsets the fuel saving, cost for introduction and maintenance, environment resistance, difficulty in maintenance and so on. As for attempt of application of riblets to commercial aircraft, 2% reduction of total air drag was confirmed by Airbus A320 flight test, which corresponds to an annual saving of more than 50000 litters' fuel consumption per aircraft in normal regular service (MBB Transport Aircraft Group, 1988). Generally, about 8% reduction of turbulent skin friction drag can be achieved with well-designed riblet.

Bechert et al. (1997) concluded from their experiments that "blade riblets," which is like row of thin fences along streamwise direction, is optimal as 2D configuration. On the other hand, effectiveness of 3D riblets has been discussed (Viswanath, 2002; Pollard, 1997). Several streamwise variations of configurations have been analyzed as 3D riblets, such as zigzag, (Japan Atomic Energy Agency, 2002; Sha et al., 2005), sinusoidal, (Peet et al, 2008; Peet et al., 2012; Grüneberger, 2012) and the others (Bechert et al., 1997a; Wilkinson et al., 1988; Bruse, 1993; Miki et al., 2011). While several streamwise variations of configurations have been analyzed as 3D riblets, sinusoidal riblets in particular are reported to be more effective than straight riblets (Peet et al., 2008; Peet et al., 2012).

Authors conducted DNS of flow over both straight and sinusoidal riblets (Yamada et al., 2013). It was confirmed from computed instantaneous field and results of quadrant analysis that well-known drag reduction mechanism of straight riblet is also reproduced over sinusoidal riblets; Friction drag is reduced because down-wash cannot reach the riblet grooves. In previous research by Peet et al. (2008), turbulence statistics over sinusoidal riblet is investigated aiming at examining improvement process of drag reduction by sinusoidal shape. However, the mechanism is not yet clarified. On the other hand, it seems from our previous research (Yamada et al., 2013) that friction drag on wetted area is closely related instantaneous flow field inside the riblet grooves. In this study, therefore, instantaneous flow field inside the riblet grooves are investigated to examine the improvement process caused by sinusoidal shape.

1 OUTLINE OF COMPUTATION

1.1 Computational Condition

Objective of analysis is the channel flow which has flat surface on upper wall and riblet surface on lower wall. Figure 1 is an example of computational domain. Sinusoidal curves of riblets are specified by wavelength λ and ampli-

Table 1. Computational condition for DNS of channel turbulence with riblets.

	Re_τ	tips	Grid point			Domain		
		N_{tips}	N_x	N_y	N_z	L_x	L_y	L_z
flat plate	180	-	256	128	256	$4\pi\delta$	2δ	$2\times 0.289\pi\delta$
$s^+ = 20$ (except $\lambda^+ = 1508$)	180	16	256	128	512	$4\pi\delta$	2δ	$2\times 0.289\pi\delta$
$s^+ = 40$	180	8	256	128	512	$4\pi\delta$	2δ	$2\times 0.289\pi\delta$
$\lambda^+ = 1508$	180	16	344	128	512	$16/3\pi\delta$	2δ	$2\times 0.289\pi\delta$

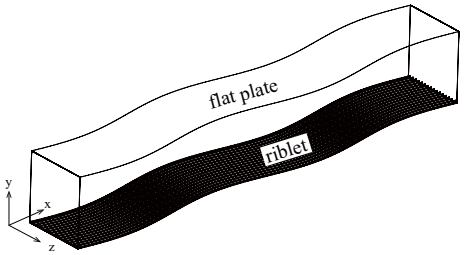

Figure 1. Computational domain for flows over wavy riblets.

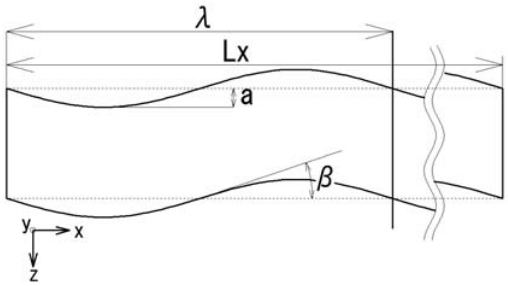

Figure 2. Top view of configuration of wavy riblets.

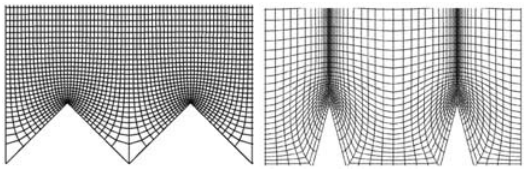

(a) trianglar (b) trapezoidal

Figure 3. Cross-sectional computational mesh near riblets.

tude a as shown in Fig. 2. Sinusoidal curves are also specified by λ and angle β (Peet et al., 2008; Peet et al., 2012), which is defined as

$$\beta = tan^{-1}\left(2\pi\frac{a}{\lambda}\right), \tag{1}$$

also shown in Fig. 2. For the convenience of organizing the computational results, each case is set by combination of wavelength λ and angle β. As $y-z$ cross-section, triangle and trapezoidal cross-section is adopted. Trapezoidal riblet is proposed as a suboptimal shape considering the introduction to aircraft (Bechert et al., 1997). Figure 3 represents computational mesh for trapezoidal riblet. Riblet height h is set to be half of spanwise spacing of grooves s, which is confirmed to be effective size (Yamada et al., 2013). All the computational cases will be shown later together with the calculated drag reduction rates. Table 1 represents the detailed information of computational domain. Wall unit of riblet spacing, s^+, and grid points on each spacing are same as those of Choi et al. (1993) for comparison. Streamwise length of computational domain, on the other hand, is set to be 4 times as long as Choi et al. (1993), because test calculation shows that streaks are found to be longer than original domain length. Spanwise length is set to be 2 times as long as Choi et al. (1993) so that interaction of turbulence structure can be fully observed. Pressure gradient of streamwise direction $\partial P/\partial x = -1$ is applied as driving force. Reynolds number Re_τ, which is based on the wall-shear velocity of the flat plate $u_{\tau f}$ and the channel half-width δ, is set to be 180 to compare with each previous result (Choi et al., 1993).

1.2 Numerical Method

The method of unsteady direct numerical simulation is based on the fractional step method for incompressible flow. The convective term and viscous term are discretized by central finite difference of 2nd order accuracy. Adams-Bashforth method of 2nd order accuracy is applied for time marching of these terms. The periodicity is assumed in the streamwise (x) and spanwise (z) direction.

The code was validated by comparing with DNS result of two-flat-plate channel by Kim et al. (1987) and also comparing with experimental and DNS results of flow over triangle-grooved riblets (Walsh, 1982; Choi, 1993).

These calculations were performed on JAXA Supercomputer System (JSS).

2 DRAG REDUCTION RATE

2.1 Definition

Friction drag reduction rate DR_f is defined as

$$DR_f = \frac{D_{f\,riblet} - D_{f\,flat}}{D_{f\,flat}} \tag{2}$$

where D_f is friction drag which is calculated by

$$D_f = -\mu\int_A \frac{\partial u}{\partial n} dA. \tag{3}$$

Here, n is normal vector on wetted surface and A is wetted area. Subscript *riblet* represents 'riblet surface (lower side of domain)', $flat$ represents 'flat surface (upper side of domain)', respectively. Not only friction drag but also pressure drag occurs on sinusoidal riblet. Total drag D is defined as sum of friction drag D_f and pressure drag D_p:

$$D = D_f + D_p$$

Table 2. Calculated drag reduction rates. (*: experiment by Walsh (1982), **: DNS by Choi et al. (1993), †: experiment by Bechert et al. (1997))

case	cross -section	streamwise	wave length λ^+	amplitude a^+	angle β	spacing s^+	Friction drag reduction rate	Total drag reduction rate
tri-s20	triangle	straight	-	-	-	20	-2.8% (-3%*, -5%**)	←
tri-s40	triangle	straight	-	-	-	40	+3.3% (+3%*, +2%**)	←
trap	trapezoid	straight	-	-	-	20	-6.1% (-7.6%†)	←
trap-λ^+1508-β10.7	trapezoid	sine	1508	45	10.7	20	-9.7%	-7.2%
trap-λ^+1131-β32.1	trapezoid	sine	1131	113	32.1	20	-15.5%	+10.0%
trap-λ^+1131-β21.7	trapezoid	sine	1131	68	21.7	20	-11.4%	-1.6%
trap-λ^+1131-β10.7	trapezoid	sine	1131	34	10.7	20	-10.3%	-7.8%
trap-λ^+565-β10.7	trapezoid	sine	565	17	10.7	20	-8.7%	-5.9%
trap-λ^+283-β10.7	trapezoid	sine	283	8.5	10.7	20	-10.5%	-7.4%
trap-λ^+1131-β5.7	trapezoid	sine	1131	18	5.7	20	-7.0%	-6.3%

$$= \int_A \left(-\mu \frac{\partial u}{\partial n} + P_w n_x\right) dA. \quad (4)$$

Here, P_w is pressure above wetted surface and n_x is streamwise component of normal vector. Same as DR_f (eq. (2)), total drag reduction rate is defined as

$$DR_{total} = \frac{D_{riblet} - D_{flat}}{D_{flat}}. \quad (5)$$

2.2 Summary of Parametric Analysis

Calculated drag reduction rates are shown in Table 2. Drag reduction rate of triangle cross-section (tri-s20 and tri-s40) are compared with experimental results of Walsh (1982) and DNS results of Choi et al. (1993). They reported that variation of drag reduction rate are $\pm 1\%$ and $\pm 2\%$ respectively. Our results are reasonable considering these variations. Drag reduction rate of straight riblet with trapezoidal cross-section (trap) is in good agreement with experimental results of Bechert et al. (1997).

Figure 4 represents drag reduction rate for various $\tan\beta$. Friction drag reduction rate is improved by each sinusoidal riblet compared with that of straight riblet ($\tan\beta = 0$). Total drag (friction drag + pressure drag) reduction rates are also improved in some cases at a maximum reduction rate of -7.8%, while reduction rate of straight riblet is -6.1%.

Figure 4 shows that the larger the β is, the better friction drag reduction rate gets. On the other hand, total drag reduction rate get worse except for 3 cases of $\beta = 10.7°$. Particularly, total drag reduction effect is lost with $\beta = 32.1°$. Solid lines in Fig. 4 represent approximated curves obtained from calculation point. Friction drag reduction rate drops in direct proportion to $\tan\beta$ and pressure drag rate (pressure drag/friction drag of flat surface) increases directly with the square of $\tan\beta$. These agree with the computational results of flow over sinusoidal riblets reported by Peet et al. (2012). From approximated curves of total drag reduction rate (green line + black line), $\tan\beta \approx 0.1 (\beta = 5.7°)$ seems to be the most effective parameter. With $\beta = 5.7°$ and $\lambda^+ = 1131$, however, calculated total drag reduction rate is not the best among all the cases. This may be attributed to the slight difference of friction drag caused by value of λ, while pressure drag is determined mostly by β (discussed later).

The cases with various wavelength λ and same β are compared. Figure 5 represents drag reduction rate for various λ^+ with same β(=10.7°). This figure shows that difference between various λ is slight compared with that between various β (Note that vertical axis is different from Fig. 4). These small differences, however, are important for search of the optimal value. In Fig. 5, total drag reduction rate are the smallest at $\lambda^+ = 1131$ among the four cases. Peet et al. (2012) predicted that the most effective wavelength is $\lambda^+ \sim 1000$. They concluded that λ^+ which is larger or smaller than 1000 disrupts self-maintenance cycle of turbulence in wall flows, which is to increase drag; Characteristic scale of turbulence, such as advection distance of streamwise vortex before breakup or length of low-speed streak, is about 1000 in wall-unit. Our results show that the smallest drag reduction rate is certainly obtained at about $\lambda^+ = 1000$ as Peet et al. (2012) predicted. However, these four data points cannot infer local minimum is at about $\lambda^+ = 1000$.

Pressure drag seems to be determined mostly by β because difference of pressure drag among various wavelength is much smaller than that among various β.

3 DISCUSSION ABOUT IMPROVEMENT OF DRAG REDUCTION EFFECT

In this section, all the trapezoidal cases and case of two-flat-plate channel are compared to examine the mechanism of improved drag reduction effect by sinusoidal shape.

Figure 6(a), (b) represent instantaneous distribution of w, u and $\mu \partial u/\partial n$ (streamwise component of wall shear stress), along one of the grooves, respectively. Figure 7 are the power spectra obtained by subjecting spatial distributions of w, u and $\mu \partial u/\partial n$ to FFT processing, i.e. examples

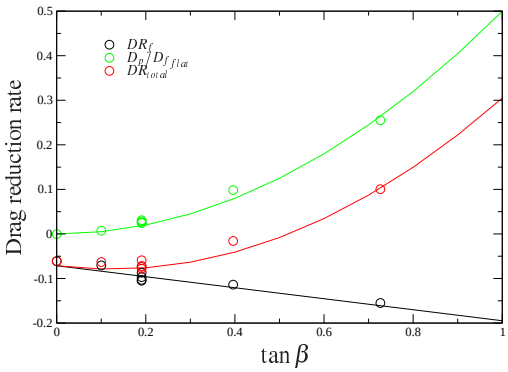

Figure 4. Drag reduction rates versus $tan\beta$ (symbol: present results, lines: fitting curves).

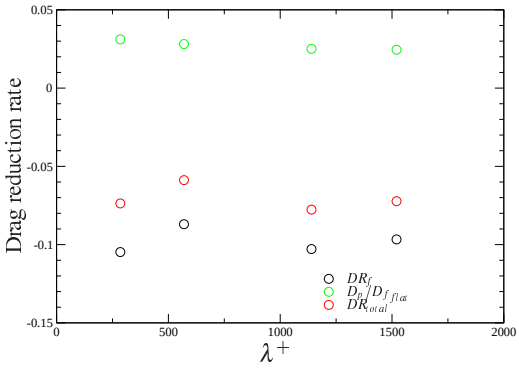

Figure 5. Drag reduction rates versus $\lambda^+(\beta = 10.7°)$.

of the sample data of FFT are Fig. 6. Figure 6(a) shows that amplitude and wavelength of fluctuating spanwise velocity w are corresponding to those of sinusoidal riblets. In Fig. 7(a), peak value of power spectra of w are represented at the wave number $1/\lambda$ which determine respective sinusoidal shapes. Harmonic is also detected in case trap-λ^+1131-β32.1. In Fig. 6(b), strong correlation between streamwise velocity u and streamwise component of wall shear stress $\mu\partial u/\partial n$ is observed. In sinusoidal case, $\mu\partial u/\partial n$ is smaller at the position where reverse flow (negative u) occurs. Particularly in case trap-λ^+1131-β32.1, many reverse flows occur, which corresponds to the significant improvement of friction drag reduction rate shown in Table 2.

Figure 8 shows 3 examples of instantaneous flow field. Upper and lower figures represent vortical structure inside the grooves and streamwise component of wall shear stress $\mu\partial u/\partial n$, respectively.

In Fig. 8(a), spanwise vortices occur periodically at the phase where angle between flow and riblet tip is the largest. Spanwise vortices occur by separation from riblet tip as shown in Fig. 9. Reverse flow in the vicinity of the riblet surface makes $\mu\partial u/\partial n$ negative. In the lower figure of Fig. 8(a), the areas where $\mu\partial u/\partial n$ are particularly small correspond with spanwise vortices. This is confirmed also by power spectra. In Fig. 6(b) and (c), peak is clearly detected only in case trap-λ^+1131-β32.1 and trap-λ^+1131-β21.7. The wave number at which peak is represented is twice the wave number of sinusoidal shape. This implies that separation and reverse flow occur at the phase where angle between flow and riblet tip is the largest.

If angle β is relatively small(Fig. 8(b)), on the other hand, occurrence of spanwise vortices is not so periodic as that of the cases of $\lambda^+ = 1131$, $\beta = 32.1°$(Fig. 8(a)). Thus peak is not clearly detected in Fig. 6(b) and (c). Spanwise vortices occur also above straight riblet as shown in Fig. 8(c), the cause of which is not clarified yet. Nonetheless, even if angle β is relatively small, friction drag reduction effect is improved from straight riblet, because more spanwise vortices occur from sinusoidal riblet tips. Total drag reduction effect is also improved in 4 cases. In those cases, pressure drag increasing effect is smaller than friction drag reducing effect. The most effective β obtained from the parametric study is determined from trade-off between friction drag reduction effect and pressure drag increasing effect of β.

4 CONCLUSION

DNS results of flow over sinusoidal riblets were analyzed to investigate improvement mechanism of drag reduction effect. This can be summarized as follows:

1. Total drag (pressure drag + friction drag) reduction rate of sinusoial riblet is improved in some cases at a maximum reduction rate of -7.8%, while reduction rate of straight riblet is -6.1%.
2. Friction drag reduction rate drops in direct proportion to $\tan\beta = 2\pi a/\lambda$ (a: amplitude, λ: wavelength) and pressure drag rate (pressure drag/friction drag of flat surface) increases directly with the square of $\tan\beta$.
3. If angle β is relatively large, flow is separated from riblet tips. Spanwise vortices which occur periodically by the separation reduce friction drag. Regarding reduction of total drag, trade-off between β and pressure drag should be considered. If angle β is relatively small, spanwise vortices occur less frequently and not periodically. Nonetheless, considering total drag reduction, relatively small β seems better because pressure drag increasing effect is smaller than friction drag reducing effect.
4. Difference of friction drag among various λ, on the other hand, is slight compared with that among various β. These small differences, however, are important for search of the optimal value. Pressure drag also seems to be determined mostly by β because difference of pressure drag among various wavelength is much smaller than that among various β.

REFERENCES

Bechert, D. W., Bruse, M., Hage, W. , van der Hoeven, J. G. T. and Hoppe, G., 1997, "Experiments on Drag-reducting Surfaces and their Optimization with an Adjustable Geometry", J.Fluid Mech, vol.338, pp. 59-87.

Bechert, D. W., Bruse, M., Hage, W. and Meyer, R., 1997a, "Biological Surfaces and their Technological Application -Laboratory and Flight Experiments on Drag Reduction and Separation Control", Proc. of 28th AIAA Fluid Dynamics Conference, AIAA-1997-1960.

Bruse, M., Bechert, D. W., Th van der Hoeven, J. G., Hage, W. and Hoppe, G., 1993, "Experiments with Conventional and with Novel Adjustable Drag-reducing Surfaces", In: So, R. M. C., Speziale, C. G. and Launder, B. E. (Editors) Near wall turbulent flows, Amsterdam: Elsevier Science Publishers, pp. 719-738.

Choi, H., Moin, P. and Kim, J., 1993, "Direct Numerical Simulation of Turbulent Flow over Riblets", J. Fluid Mech., Vol. 255, pp. 503-539.

Grüneberger, R., Kramer, F., Wassen, E., Hage, W., Meyer, R. and Thiele, F., 2012, "Influence of Wave-Like

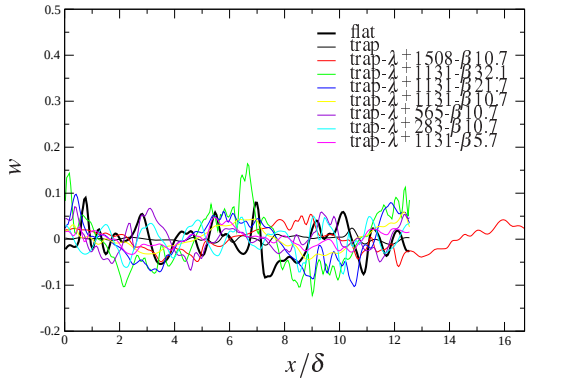

(a) w

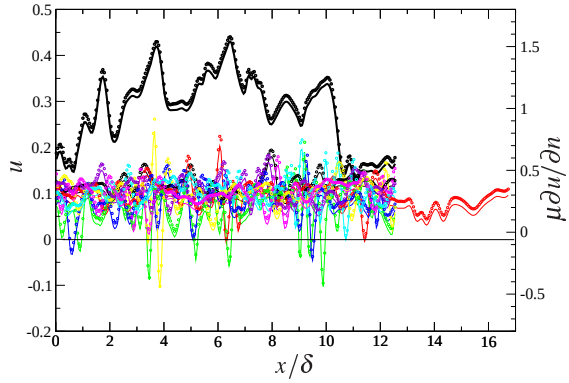

(b) u and $\mu\partial u/\partial n$ (solid: u, symbol: $\mu\partial u/\partial n$, legend is same as (a))

Figure 6. Instantaneous velocity and wall shear stress along a groove.

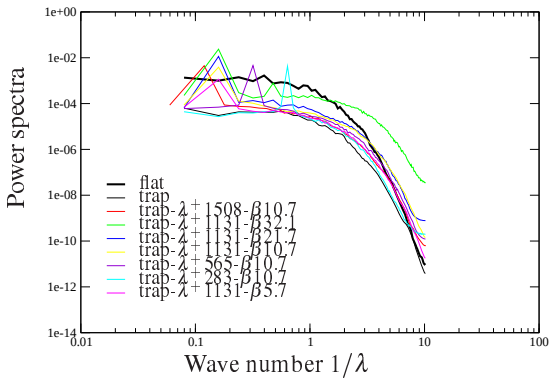

(a) w

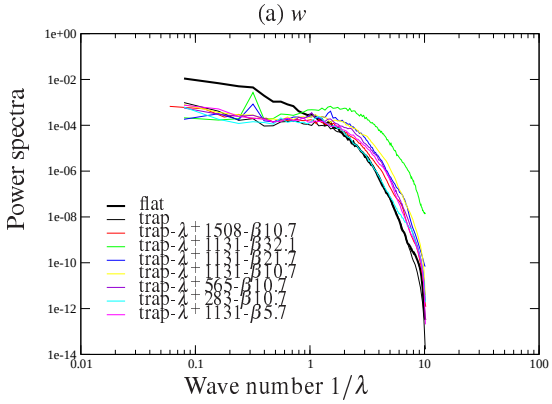

(b) u

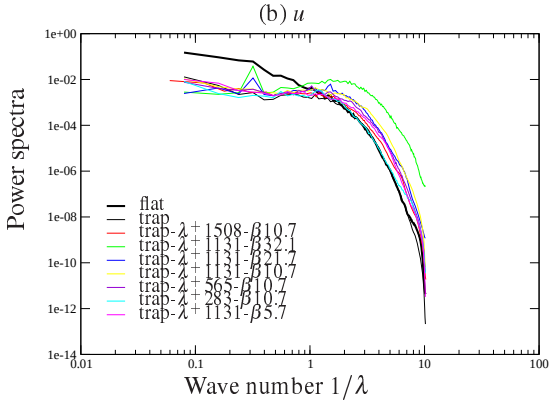

(c) $\mu\partial u/\partial n$

Figure 7. Power spectra of spatial fluctuation along bottom of riblet.

Riblets on Turbulent Friction Drag", Nature-Inspired Fluid Mechanics, Vol. 119, pp. 311-329.

Japan Atomic Energy Agency (formerly Japan Atomic Energy Research Institute), 2002, "Turbulent Friction Drag Reducing Surface" (in Japanese), Japanese Patent, P2002-266816A, 2002-09-18.

Kim, J., Moin, P. and Moser, R., 1987, "Turbulence Statistics in Fully Developed Channel at Low Reynolds Number", J. Fluid Mech., Vol. 177, pp. 133-166.

MBB Transport Aircraft Group, 1988, "Microscopic Rib Profiles Will Increase Aircraft Economy in Flight", Aircraft Engineering, Vol. 60, No. 1, pp. 11.

Miki, H., Iwamoto, K. and Murata, A., 2011, "PIV Analysis on a 3-Dimensional Riblet for Drag Reduction" (in Japanese), Transactions of the Japan Society of Mechanical Engineers Series B, Vol. 77, No. 782, pp. 25-36.

Peet, Y. and Sagaut, P., 2008, "Turbulent Drag Reduction Using Sinusoidal Riblets with Triangular Cross Section", Proc. of the 38th AIAA Fluid Dynamics Conference and Exhibit, No. AIAA-2008-3745.

Peet, Y., Sagaut, P. and Charron, Y., 2012, "Pressure Loss Reduction in Hydrogen Pipelines by Surface Restructuring", Int. J. of Hydrogen Energy, Vol. 34, pp. 8964-8973.

Pollard, A., 1997, Passive and Active Control of Near-wall Turbulence, Progress in Aerospace Sciences, Vol. 33, pp. 689-708.

Sha, T., Itoh, M., Tamano, S., Yokota K., and Akino N., 2005, "Experimental Study on Drag Reduction in Turbulent Flow on Zigzag Riblet Surface" (in Japanese), Proc. of the 88th Fluid Engineering Division Conference of the Japan Society of Mechanical Engineers, No. 207.

Stenzel, V., Wilke, Y. and Hage, W., 2011, "Drag-reducing Paints for the Reduction of Fuel Consumption in Aviation and Shipping", Progress in Organic Coating, Vol. 70, pp. 224-229.

Viswanath, P. R., 2002, "Aircraft Viscous Drag Reduction Using Riblets", Progress in Aerospace Sciences, Vol. 38, pp. 571-600.

Walsh, M. J., 1982, "Turbulent Boundary Layer Drag Reduction Using Riblets ", AIAA Paper 82-0169.

Wilkinson, S. P., Anders, J. B., Lazos, B. S. and Bushnell, D. M., 1988, "Turbulent Drag Reduction Research at NASA Langley - Progress and Plans", Int. J. of Heat and Fluid Flow, Vol. 9, No. 3.

Yamada, Y, Okabayashi, K. and Asai, M., 2013, "Numerical Analysis on Improvement of Wavy Riblets" (in Japanese), Proc. of the Annu. Meeting of Japan Society of Fluid Mechanics 2013, No. 122, pp. 1-6.

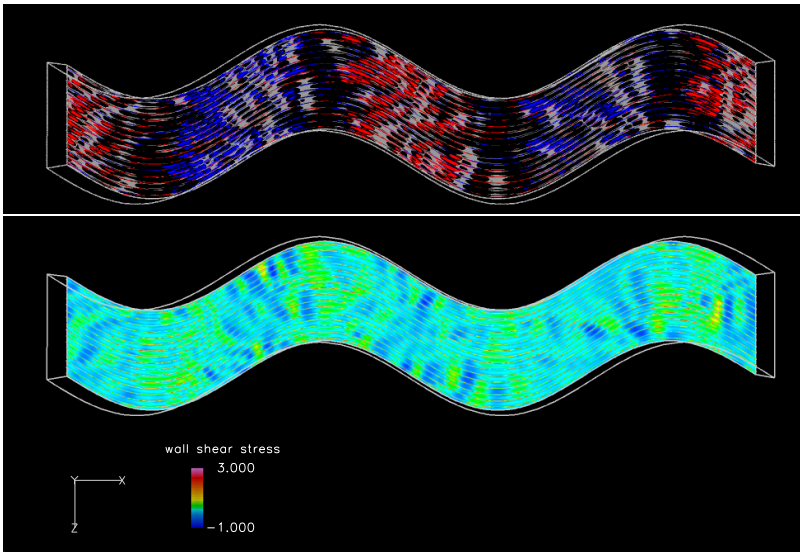

(a) trap-λ^+1131-β32.1

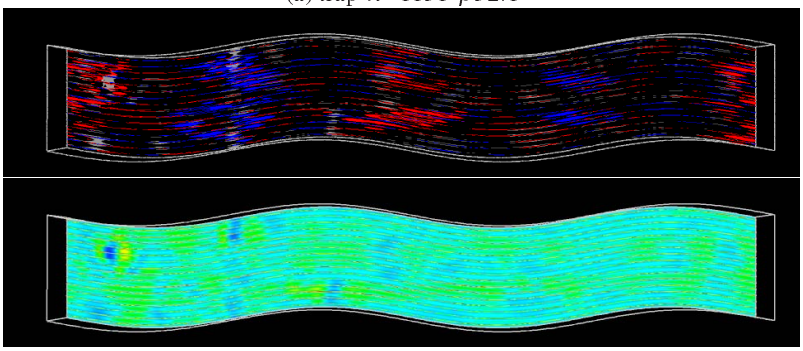

(b) trap-λ^+1131-β10.7

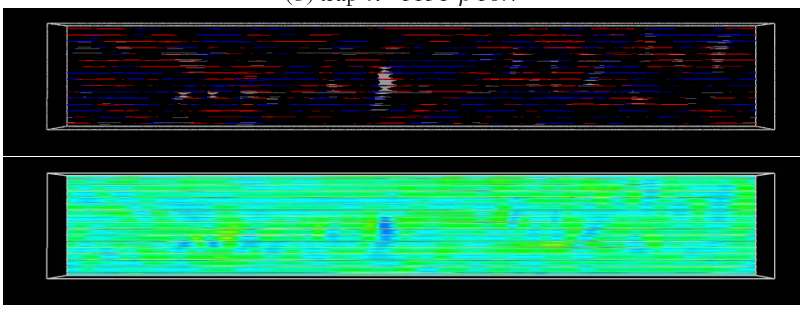

(c) trap

Figure 8. Instantaneous vortical structure and streamwise component of wall shear stress (red: streamwise vorticity $\omega_x = 20$ ($\omega_x = 40$ only for (a)), blue: $\omega_x = -20$($\omega_x = -40$ only for (a)), gray: $\omega_z = -10$, contours: $\mu \partial u/\partial n$).

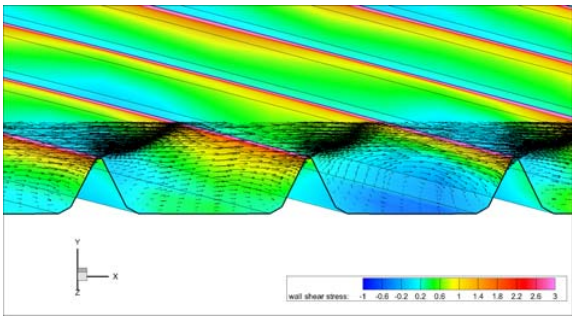

Figure 9. An example of instantaneous velocity vector at separating region.